Supplemental Data

Functional Reconstitution

of ESCRT-III Assembly and Disassembly

Suraj Saksena, Judit Wahlman, David Teis, Arthur E. Johnson, and Scott D. Emr

Supplemental Results

S.i. Cysteine Substitutions Do Not Interfere With the Stability and/or Function of Vps20 & Snf7

To ensure that the cysteine substitutions introduced in Vps20 and Snf7 for NBD labeling did not interfere with the folding, stability and cellular function of the protein, we monitored the vacuolar sorting of the MVB cargo GFP-CPS in cells expressing cysteine mutants of Vps20 and Snf7. As shown in Fig. S1, GFP-CPS was sorted normally to the vacuolar lumen in cells expressing Snf7 E81C and Snf7 K215C. Similarly, normal sorting of GFP-CPS was seen in cells expressing Vps20 K61C and Vps20 S190C. In addition, we found that each of the nine Snf7 cysteine mutants and the four Vps20 cysteine mutants reported here do not interfere with the vacuolar sorting of GFP-CPS (data not shown).

S.ii. Vps20 Residues Are Exposed to the Nonpolar Core of the Bilayer

NBD probes attached to Vps20 could move into a nonpolar environment either by becoming exposed to the nonpolar interior or interface of the bilayer, or by moving into an intra- or inter-protein hydrophobic cleft or surface. To discriminate between these two possibilities, the most direct approach is to bind the protein to liposomes containing a collisional quenching moiety that is restricted to the nonpolar core of the bilayer. When an excited NBD dye contacts a nitroxide (NO) moiety, the NBD excitation energy is dissipated without the emission of a photon. Thus, collisions between NO groups and NBD reduce the emission intensity of a sample. By covalently attaching an uncharged NO group to carbon-5 of a PC acyl chain to form 5-NO-PC, the quencher is spatially restricted to the nonpolar core of the bilayer. This approach therefore directly determines whether an NBD dye is exposed to or embedded in the interior of the membrane, since sample intensity will decrease only if the NO can access and collide with the NBD (Johnson, 2005; Shatursky et al., 1999). On the other hand, it is important to note that the NBD dye is tethered to the polypeptide backbone by a flexible covalent linkage that is more than 11 Å long. Hence, the dye may extend beyond the normal protein surface and be dynamically exposed to the membrane interior when the protein is peripherally associated with the membrane surface.

To test whether the NO lipid modification of liposomes had any effect on their protein-binding ability, a sample of $Vps20^{61\text{-}NBD}$ was incubated with liposomes containing 5-NO-PC, and then purified by gel filtration chromatography. Since essentially all of the NBD fluorescence was found to co-elute in the void volume

with the liposomes (detected by light scattering) and very little eluted with free Vps20 assayed in the absence of liposomes (Fig. S3A), more than 95% of the $Vps20^{61\text{-}NBD}$ was bound to liposomes after elution. Furthermore, the binding curve obtained upon titration of $Vps20^{61\text{-}NBD}$ with 77.5 mole% PC/PS/PI/22.5 mole% 5-NO-PC (data not shown) was identical to the binding curve obtained upon titration of $Vps20^{61\text{-}NBD}$ with PC/PS/PI (Fig. 1C). These data strongly indicate that the NO lipid modification has no measurable effect on the protein-binding ability of the liposomes.

When either $Vps20^{61\text{-}NBD}$ or $Vps20^{190\text{-}NBD}$ was titrated with liposomes containing 5-NO-PC, the NBD emission intensity was reduced substantially (Figs. S3B-S3F). Thus, NBD dyes at 61 and 190 must be exposed to the nonpolar membrane interior where the NO group can contact the NBD dye. These observations are also consistent with the large intensity increases that occur upon membrane binding (Fig. 1E). Furthermore, the extent of quenching increased as the 5-NO-PC concentration increased because the frequency of NBD collisions with NO was then increased. These collisional quenching data therefore show directly that the binding of Vps20 to the membrane surface involves two residues (61 and 190) that are well-separated in the homologous hVps24 crystal structure (Fig. 1F). Furthermore, Vps20 association is apparently promoted by hydrophobic interactions between the membrane and the protein near those residues.

In contrast, the NBD at position 170 is not exposed to the membrane interior because it is poorly quenched by 5-NO-PC (Fig. S3D). The probe at residue 7 is exposed to the NO group (Fig. S3D), but the extent of quenching, and hence the frequency of NBD-NO collision, is significantly reduced compared to the quenching of probes at 61 and 190. Hence, the accessibility of the dye at residue 7 to the NO moieties is more limited.

S.iii. Snf7 Residues Are Exposed to the Nonpolar Membrane Interior

When either $Snf7^{81\text{-}NBD}$ or $Snf7^{200\text{-}NBD}$ was titrated with liposomes containing 5-NO-PC, the NBD intensity was reduced substantially (Fig. S5A,B). The NBD dyes at residues 81 and 200 must therefore be exposed to the nonpolar core of the membrane bilayer where the NO group can contact and quench the NBD dye. Exposure of these dyes to the lipid phase is also consistent with their intensity increases and $\lambda_{em\ max}$ decreases experienced upon membrane binding (Fig. 3C). In contrast, the NBD at position 14 is not exposed to the membrane interior because it is poorly quenched by 5-NO-PC (Fig. S5C). NBD probes at three other Snf7 sites were also quenched by the NO moieties (Fig. S5C). Thus, several sites and surfaces along the entire length of Snf7 contact the nonpolar interior of the bilayer upon binding to the surface (Fig. 3D).

S.iv. The α5-α6 Loop and Key Residues In and Around α4 are Directly Involved in Snf7 Oligomerization and Function

We have shown by collisional quenching that residues in the polypeptide loop between helices α5 and α6 of both Vps20 and Snf7 become exposed to the nonpolar interior of the bilayer upon binding to the membrane (Fig. S3, S5).

Since the movement from an aqueous to nonaqueous milieu seems likely to involve a conformational change for this portion of the Vps20 and Snf7 molecules, we made some mutations in this region of the protein to assess its sensitivity to membrane binding and interactions with other proteins. Examination of the Snf7 sequence revealed the presence of three prolines (Pro191, Pro200 and Pro203) at the junction of α5 and the loop leading to α6 (Fig. S9), and Vps20 has three proline residues at this junction site.

To ascertain whether these proline residues play an important role in Snf7 oligomerization and function, the triple proline mutant of Snf7 (P191W P200W P203W), hereafter referred to as the Snf7 PW mutant, was expressed in cells on the expectation that the bulky tryptophans would restrict conformational rearrangements of the loop and the movement of α6. *snf7Δ* cells expressing the Snf7 PW mutant were compromised in their ability to sort GFP-CPS, a cargo that is normally sorted into the vacuolar lumen via the MVB sorting pathway (Fig. 5D). In contrast, GFP-CPS was sorted normally to the vacuolar lumen in wild type cells (expressing wild type Snf7 and Vps20) (Fig. 5D). Similarly, *vps20Δ* cells expressing the Vps20 PW mutant (P183W P189W P192) were compromised in their ability to sort GFP-CPS to the lumen of the vacuole because GFP-CPS was mislocalized to the limiting membrane of the vacuole (Fig. 5D).

To determine at what stage Snf7 function was inhibited, the PW mutations were examined in vivo using the same approach used in the in vitro experiments described here. When ESCRT-III disassembly is blocked by using a *vps4Δ* strain, ESCRT-III (Snf7 and other ESCRT-III proteins) accumulates as a high molecular weight (440-600 kDa) endosome-associated (P13 fraction) complex that sediments at the bottom of a glycerol velocity gradient (Fig. 5E)(Teis et al., 2008). However, a similar experiment performed using *vps4Δsnf7Δ* cells expressing the Snf7 PW mutant revealed that the mutant form of Snf7 was unable to oligomerize into a high molecular weight complex that sediments at the bottom of the gradient (Fig. 5E). The inability of the Snf7 PW mutant to oligomerize was also shown in vitro by glycerol gradient sizing (Fig. 5Cxi) and by FRET experiments: no FRET was detected even in the presence of excess liposomes and Vps20 (TableS1). The combined results reveal that the α5-α6 loop is required for Snf7 oligomerization, and this oligomerization is essential for the sorting function of Snf7.

We recently demonstrated that soluble Vps24 forms filament-like structures in vitro and identified key residues in α4 and the loop linking α3 to α4 that mediate monomer-monomer contacts in the Vps24 filament (Ghazi-Tabatabai et al., 2008). Since Snf7 contains identical or similar residues at these sites (Fig. S9), the effect of mutating these key residues on Snf7 oligomerization was examined by generating two point mutants of Snf7 ($Snf7^{L121D}$ and Snf7 R134E E135R; hereafter referred to as $Snf7^{RE}$ mutant). As with the $Snf7^{PW}$ mutant, the two point mutants of Snf7 were impaired in oligomerization both in vitro (Fig. 5Cix,x) and in vivo (Fig. 5E), and consequently, in sorting GFP-CPS to the vacuolar lumen (Fig. 5D).

S.v. Vps20 Myristoylation is Not Critical for Snf7 Recruitment to Endosomes and Snf7 Oligomerization in vivo

Vps20 contains a recognition sequence for the enzyme myristoyl-CoA:protein *N*-myristoyltransferase Nmt1 that is responsible for covalent attachment of a myristoyl group to the N-terminal glycine of target proteins. Since the recombinant Vps20 in our in vitro assays (spectroscopic and non-spectroscopic) is not myristoylated, we wanted to test whether a non-myristoylated form of Vps20 expressed in yeast is capable of performing the key functions of Vps20 suggested by our in vitro data i.e. recruiting Snf7 to endosomes and nucleating Snf7 oligomerization. To this end, we monitored Snf7 recruitment to endosomes, and Snf7 oligomerization on endosomes in a *Δvps20* strain expressing a mutant form of Vps20 (G2A), in which the N-terminal glycine is modified to alanine and hence the protein is not myristoylated. Interestingly, the G2A mutant of Vps20 was able to recruit Snf7 to endosomes as efficiently as wild type Vps20 (data not shown). More importantly, the G2A mutant was efficient in nucleating Snf7 oligomerization on endosomes. Velocity sedimentation experiments performed using *vps4Δvps20Δ* cells expressing the Vps20 (G2A) mutant revealed that Snf7 oligomerizes into a high molecular weight complex that sediments at the bottom of the gradient (Fig. S10). These results explain the fact that the GFP-CPS sorting defect observed in cells expressing the Vps20 (G2A) mutant is less severe than in a *Δvps20* strain (Babst et al., 2002). Based on the highly basic character of the helix α1 in Vps20 and other ESCRT-III proteins, we predict that Vps20 binding to liposomes in our assays is in large part electrostatic in nature. The myristoylation modification in vivo may help provide additional binding energy to stabilize Vps20 association with membranes and/or to anchor Vps20 at a specific site on the endosome that orients it appropriately for interactions with ESCRT-II. However, the modification is apparently not necessary for the downstream functions of Vps20 such as membrane recruitment of Snf7 and nucleation of Snf7 oligomerization.

S.vi. Changes in the Spectral Properties of NBD are a Direct Readout for Conformational State

Movement of an NBD dye from an aqueous milieu to a hydrophobic environment is accompanied by a change in its spectral properties (e.g. emission intensity, fluorescence lifetime, anisotropy etc.). To directly test if we could visualize two different conformational states of an ESCRT-III protein by monitoring changes in the spectral properties of NBD, we purified two mutants of Snf7 each of which lacked the loop linking helix α5 and α6 (hereafter referred to as Snf7 loop mutants). We labeled one Snf7 loop mutant at position 81 with NBD by introducing a cysteine at residue 81, and the second loop mutant was labeled at position 93 by introducing a cysteine at residue 93. We then compared the NBD emission of wild type Snf7 labeled at residues 81 and 93 with the NBD emission of the Snf7 loop mutants labeled at residues 81 and 93. These comparisons were made using sample amounts that normalized the protein concentration and the NBD-labeling efficiency of the two different samples being compared.

We found that the NBD emission intensity of the loop mutant labeled at residue 81 was half the intensity observed for the wild type protein (Fig. S11). More strikingly, the NBD emission intensity of the loop mutant at residue 93 was a quarter of the intensity observed for the wild type protein (Fig. S11). In addition, both the loop mutants exhibited a different fluorescence lifetime and anisotropy compared to their wild type counterparts (data not shown). As shown in Fig. S11, these differences can be explained by the fact that deletion of the autoinhibitory loop unmasks helix α2, thereby making the NBD dye more water exposed. These data directly demonstrate the sensitivity of NBD emission to its environment and highlight the value of this technique in monitoring conformational rearrangements in proteins.

Supplemental Discussion

Spectroscopic Examination of Conformational Rearrangements in Vps20 and Snf7

The spectroscopic characterization of Vps25 interactions with NBD-labeled Vps20 revealed three results that were unexpected based on previous work. First, a previous study reported that recombinant Vps25 binds to Vps20 in solution using a pull-down assay (Teo et al., 2004). Yet at the protein concentrations used in our assays, Vps25 has low to no spectroscopically detectable affinity for Vps20 in solution (Fig. 2A-C;S4B), but a high affinity for membrane-bound Vps20 (Fig. 2D-F). Second, the same study reported that Vps20 binding to Folch liposomes was dramatically increased upon addition of Vps25 (Teo e al., 2004). Yet at the protein concentrations and liposome concentration and composition used in our assays, we observed efficient binding of Vps20 to PC/PS/PI without Vps25 addition (Fig. 1C,D;S2). Furthermore, we found that addition of Vps25 had no significant effect on the amount of PC/PS/PI required for Vps20 membrane-binding to go to completion (data not shown), nor did it have any effect on the amount of quenching observed for the different membrane-bound Vps20 mutants (data not shown). Thus, the Vps25-dependent increase in the emission intensity of certain NBD-labeled and membrane-bound Vps20 mutants is best explained by Vps25-induced changes in the conformation of membrane-bound Vps20 (Fig. 2D-F). Third, based on a previous report that EAP20 (ELL-associated protein 20; human orthologue of Vps25) associates with the N-terminus of CHMP6 (human orthologue of Vps20) (Yorikawa et al., 2005), it was surprising to see that the binding of Vps25 to Vps20 changed its conformation at both the N- and C-terminus. Thus, although the N-terminal domain of Vps20 undergoes a larger spectral change and perhaps a larger conformational change upon association with Vps25 (Fig. 2D-F;S4A,C), Vps25 binding clearly elicits a long-range conformational change in Vps20 that extends throughout its entire length.

The large set of NBD-labeled Vps20 and Snf7 monocysteine mutants examined here allowed us to monitor NBD emission from several sites and surfaces along the entire length of the two proteins (Fig. 1F,3D). The magnitudes

of NBD intensity changes upon membrane binding differed substantially (Fig. 1E,3C). Since the different NBD-labeled mutants exhibited similar affinities for PC/PS/PI membranes (Fig. 1C,3E,S2,S6), differences in the extents of membrane-induced changes in NBD emission most probably reflect differences in the extent to which the local environment (polar/nonpolar) of different domains is altered as a consequence of membrane binding. We also observe a good correlation between the extent of membrane-induced change in NBD emission intensity for any given site in Vps20 or Snf7 and the extent to which NBD emission from that site is quenched by membrane-restricted quenchers (compare Fig. 1E&S3D; Fig. 3C&S5C). The membrane-induced increases in NBD intensity for multiple sites along the length of Vps20 and Snf7 (Fig. 1E,3C), coupled with the quenching of the membrane-induced increases by membrane-restricted quenchers (Fig. S3B-S3F,S5A-S5C), indicate that several sites and surfaces on the two proteins (some of which are well separated in the crystal structure) contact the membrane surface.

It is important to emphasize that the existence and magnitude of a fluorescence change is determined by complex effects that are often difficult to identify precisely and unambiguously. As a result, interpretation of fluorescence data is best done by analyzing the signal using different independent techniques and correlating the results. The reduction of NBD intensity by NO quenchers can only occur if the two moieties collide. Hence, NBD quenching by NO-PC can only occur if the dye is located where the NO that is covalently attached to the acyl chain in 5NO-PC can contact the probe. The existence of quenching is therefore a diagnostic test for exposure to the membrane interior. The absence of quenching does not rule out probe exposure to the bilayer core at a location inaccessible to the NO (e.g., embedded in the bilayer but sterically protected from acyl chain NOs by other partially or fully embedded protein domains or transmembrane helices). But for peripheral membrane proteins such as the ESCRT-III proteins, the absence of quenching most likely indicates that the NBD is not exposed to the bilayer core and 5NO-PC. Increases in NBD intensity and lifetime are also indicators of probe exposure to the core because NBD intensity and lifetime are reduced by hydrogen bonding and interactions with water. Yet the close juxtaposition of certain amino acids (e.g., Cys; A. Heuck, R. Ramachandran, and A. E. Johnson, unpublished data) can also quench NBD emission. Similarly, a blue shift in the wavelength of maximum emission is frequently used to indicate NBD movement from an aqueous to non-aqueous milieu. This spectral change typically correlates with an increase in intensity, but not always, since an NBD may be quenched either before or after a transition. For example, in the case of the Vps20-190, the probe is already blue-shifted in the soluble protein ($\lambda_{em\ max}$ = 530 nm; Fig. S4B) and apparently moves to a similar non-polar environment after binding to the membrane. Hence, there is no net blue shift when this derivative binds to membranes. We therefore speculate that the intensity increase accompanying membrane-binding results from a conformational change that moves the NBD away from a residue in the folded soluble protein that quenches the probe. The collisional quenching data then

reveal that this movement exposes the NBD to the membrane interior because probe emission is reduced by 5NO-PC.

The spectroscopic examination of Snf7 interactions with other ESCRT components revealed a number of interesting insights. While we could not detect Vps20 binding to Vps25 in solution (Fig. 2A-C), Vps20 and Snf7 were found to associate both in solution and on the membrane surface (Fig.4A,B;S7B,C). Furthermore, examination of Snf7 mutants containing NBD probes at multiple locations and domains within the molecule allowed us to identify a domain of Snf7 that binds Vps20. Our data indicate that the short Snf7 α1-α2 loop and the α2 helix are sensitive to Vps20 binding both in solution and on the membrane (Fig. 4A-D; S7B-D). In contrast, Vps20 binding had no detectable effect on the probe environment and likely the conformation of the C-terminal α5-α6 loop or of α1 for either free or membrane-bound Snf7 (Fig. 4B,C;S7A,C,D). These results strongly indicate that the hetero-dimerization interactions during the assembly of the ESCRT-III lattice are mediated by interactions involving the α2 helix and the short α1- α2 loop. Our results therefore provide experimental evidence for the suggestion that ESCRT-III protein-protein association occurs at the same interface observed in the crystallized hVps24 (CHMP3) dimer (Muziol et al., 2006).

Membrane-dependent Conformational Rearrangements regulate ESCRT-III Assembly and PFO Oligomerization: Common Themes in Biology

Ligand-induced regulation of homo-oligomerization as in the case of Snf7 has been observed previously, and the best-characterized example is the cholesterol-dependent cytolysin, perfringolysin O (PFO). This water-soluble toxin binds to cholesterol-containing membranes to form oligomeric complexes that insert into the bilayer to create large aqueous pores (Heuck and Johnson, 2005). Just as oligomerization of PFO monomers is triggered by the membrane-dependent movement of a flexible loop to expose a monomer-monomer interface required for oligomer assembly (Ramachandran et al., 2004), our results strongly indicate that Snf7 oligomerization is preceded by displacement of the α5-α6 loop from the folded protein core (Fig. 3B,S5B). Consequently, mutations that compromise loop flexibility (as in the case of the Snf7 PW mutant) block Snf7 oligomerization and sorting function (Fig. 5Cxi,5D,5E; TableS1).

Supplemental Experimental Procedures

Purification & labeling of ESCRT-III proteins

Purification of Vps20 and Snf7 monocysteine mutants for NBD-labeling:

DNA encoding His-tagged Vps20 and Snf7 was cloned in pET23d (Novagen) expression vector and used as the template for PCR-based mutagenesis using QuikChange (Stratagene). All mutations were confirmed by automated DNA sequencing. The Vps20 and Snf7 mutants were expressed in C41(DE3) cells, grown at 37°C to an OD_{600nm} = 0.8, then induced with 1 mM IPTG for 4 hr at 37°C (Snf7 mutants) or 0.4 mM IPTG for 12 hr at room temperature (Vps20 mutants).

The cell pellets were resuspended in extraction buffer [50 mM HEPES (pH 8.0), 100 mM NaCl] and lysed by passage through a French pressure cell at 20,000 psi. The cell debris was removed by centrifugation at 30,000g for 15 min at 4°C. After cell lysis, the His-tagged mutants were bound to an XK 16/10 Chelating Sepharose Fast Flow column (GE Healthcare) loaded with Ni^{2+}, equilibrated in Buffer A [50 mM HEPES (pH 8.0), 100 mM NaCl, 0.05% (v/v) Triton X-100], and eluted at 3 ml/min with 300 mM imidazole, 50 mM HEPES (pH 8.0) and 100 mM NaCl.

The peak fractions from the Chelating Sepharose column were pooled and subjected to solvent exchange to get rid of imidazole. The protein solvent was changed to Buffer A [20 mM HEPES (pH 8.0), 1 mM EDTA, 1 mM DTT] by gel filtration through Sephadex G-25 (30 cm x 2.5 cm i.d.). The Vps20 and Snf7 mutant proteins were further purified by ion exchange chromatography on FPLC Q-Sepharose equilibrated in Buffer A, and eluted at 3 ml/min using a linear salt gradient (100-1000 mM NaCl in Buffer A). Following elution, the peak fractions from the ion exchange column were pooled and the protein solvent was changed to Buffer A [20 mM HEPES (pH 8.0), 1 mM EDTA, 1 mM DTT]. Purified ESCRT-III proteins were labeled with IANBD [*N,N'*-dimethyl-*N*-(iodoacetyl)-*N'*-(7-nitrobenz-2-oxa-1,3-diazolyl)ethylenediamine] or tetramethylrhodamine-5-iodoacetamide (Molecular Probes, Eugene, OR) using the same technique as described earlier (Shepard et al., 1998).The extent of covalent reaction with NBD was estimated using molar absorptivity coefficients of 5120 $M^{-1}cm^{-1}$ at 280 nm, 11,380 $M^{-1}cm^{-1}$ at 280 nm, 87,000 $M^{-1}cm^{-1}$ at 543 nm, and 25,000 $M^{-1}cm^{-1}$ at 478 nm for Vps20, Snf7, rhodamine, and NBD respectively.

The NBD-labeled Vps20 and Snf7 mutants are in a 'low salt' buffer (Buffer A) at the end of the purification scheme, which would favor them adopting their 'closed' conformation in solution (Lata et al., 2008). This was further confirmed by the fact that the purified proteins elute as a single sharp peak on a Superdex 200 sizing column (data not shown & Teis et al., 2008).

Purification of Vps24, Vps2, Vps4 and Vps4 E233Q

DNA encoding His-tagged Vps24, Vps2, Vps4 and Vps4 E233Q was cloned in pET23d (Novagen) expression vector and used as the template for PCR-based mutagenesis using QuikChange (Stratagene). All mutations were confirmed by automated DNA sequencing. Proteins were expressed in C41(DE3) cells, grown at 37°C to an OD_{600nm} = 0.8, then induced with 1 mM IPTG for 4 hr at 37°C. The cell pellets were resuspended in extraction buffer [50 mM Tris (pH 7.5), 100 mM NaCl] and lysed by sonication (Branson Sonifier 250). Lysates were cleared by centrifugation, and proteins were purified using Ni-NTA agarose (QIAGEN, Valencia, CA). After six washes in Buffer B [50 mM Tris (pH 7.5), 100 mM NaCl, 20 mM β-mercaptoethanol, 20 mM imidazole], bound proteins were eluted with Buffer C [50 mM Tris (pH 7.5), 100 mM NaCl, 20 mM β-mercaptoethanol, 250 mM imidazole]. Eluted proteins were dialyzed into Buffer A [20 mM HEPES (pH 8.0), 1 mM EDTA, 1 mM DTT] and fusion protein purity was determined by SDS-PAGE and Coomassie staining.

Gel filtration

Samples were analyzed by Sepharose CL-2B (20 cm x 1.5 cm I.D.) gel filtration chromatography, and each 1 ml fraction was eluted with Buffer D [50mM HEPES (pH 7.5) and 100mM NaCl] at 20°C and assayed for both NBD emission (λ_{ex} = 468 nm; λ_{em} = 530 nm) and 90° light scattering (λ_{ex} = 405 nm; λ_{em} = 420 nm).

FRET

After excitation by the absorption of a photon, an excited donor (D) can non-radiatively transfer its excited-state energy to a nearby acceptor (A) with the appropriate spectral properties. The excited acceptor can then emit a fluorescent photon instead of the donor. Donor emission intensity is therefore reduced by FRET, and the efficiency of energy transfer (E) is quantified most accurately by the magnitude of the A-dependent decrease in D intensity (Johnson, 2005). The magnitude of E depends primarily on the extent of overlap between the donor emission and acceptor absorption spectra, the relative orientation of the donor and acceptor transition dipoles, and – most importantly – the distance between the donor and the acceptor. The NBD-Rh donor-acceptor pair has an R_0 (the distance at which E = 50%) of ~50 Å (Turcatti et al., 1996), so E will be > 0 whenever the dyes are closer than ~100 Å ($2R_0$). One would therefore expect to detect FRET if a $Snf7^{81\text{-}NBD}$ associated with a $Snf7^{81\text{-}Rh}$ because the dyes would most likely be separated by less than 100 Å. In contrast, if Snf7 molecules remained monomeric in solution at concentrations less than 100 μM, the probes would be too far apart, on average, to detect any FRET. Thus, a significant E measurement would demonstrate the association of Snf7 proteins, either in solution or on the membrane .To measure E, four samples were prepared in parallel that differed only in the presence or absence of the donor and acceptor dyes (i.e., an equal amount of unmodified Snf7 replaced $Snf7^{NBD}$ and/or $Snf7^{Rh}$ as indicated), and they are designated D (donor-containing), DA (donor- and acceptor-containing), A (acceptor-containing), and B (a blank sample with no donor or acceptor dyes). Subtraction of the B signal from that of D corrects for the significant light scattering signal and yields the net D spectrum, while subtraction of the A signal from that of DA corrects for both the scattering and also any signal due to direct excitation of the acceptor, thereby yielding the net DA spectrum. Making the reasonable assumption that the donor dye is too far from the acceptor to alter its absorbance, E is given by $[1 – (F_{DA} - F_A)/(F_D – F_B)]$, where F is the net emission intensity of the indicated sample (Johnson et al., 1982; Mutucumarana et al., 1992; Woolhead et al., 2004).

In vitro ESCRT-III assembly assay

Purified Vps20, Snf7, Vps24 and Vps2 or various combinations of the four ESCRT-III proteins were mixed using different molar ratios and incubated with PC/PS/PI liposomes for 30 min at 22°C. Following the incubation, the liposomes were collected by centrifugation at 55,0000 rpm for 30 min. The pellet was resuspended in solubilization buffer [PBS+0.2% (v/v) Tween 20] and layered on top of a 10-40% linear glycerol gradient. In samples lacking liposomes, the

centrifugation step (described above) was omitted and the reaction sample was directly layered on top of the glycerol gradient. After layering the reaction sample on the gradient, the samples were subjected to centrifugation for 5 hr at 100,000xg. One ml fractions were collected from the top of the gradient and TCA precipitated. The gradient was calibrated for molecular sizes using the markers: aldolase, catalase, ferritin and thyroglobulin.

In vitro ESCRT-III disassembly assay

Purified Vps20, Snf7, Vps24 and Vps2 were mixed at a molar ratio of 1:10:5:3 and incubated with PC/PS/PI liposomes for 30 min at 22°C. Following the incubation, the liposomes were collected by centrifugation at 55,0000 rpm for 30 min. The pellet was resuspended in solubilization buffer [PBS+0.2% (v/v) Tween 20] and the resuspended sample was split into two fractions. One fraction was treated with Vps4 and 1mM ATP at 37°C for 45 min, while the other fraction was incubated with Vps4 and 1mM ADP at 37°C for 45 min. Following the incubation; the sample was again subjected to centrifugation at 55,000 rpm for 30 min. The pellet was resuspended in solubilization buffer [PBS+0.2% (v/v) Tween 20] and layered on top of a 10-40% linear glycerol gradient. The supernatant was also layered on top of a 10-40% linear glycerol gradient. After layering the solubilized pellet and the supernatant on the gradient, the samples were subjected to centrifugation for 5 hr at 100,000xg. One ml fractions were collected from the top of the gradient and TCA precipitated.

Microscopy

Living cells expressing fluorescent fusion proteins were grown in minimal media to an OD_{600nm} = 0.5. Cells were stained with FM4-64 as previously described for visualizing the vacuolar membrane or the class E compartment (Teis et al., 2008).

Liposome deformation assays

PC/PS/PI liposomes or PC/PS/PI liposomes treated with different proteins (ESCRT-III, ESCRT-III+Vps4+ATP, ESCRT-III+Vps4+ADP) were spotted on a formvar-coated EM grid. The samples were allowed to adsorb on the grid for 15 min at room temperature. Images were acquired following staining with 2% (w/v) uranyl acetate.

Supplemental References

Babst, M., Katzmann, D.J., Estepa-Sabal, E.J., Merloo, T., and Emr, S.D. (2002). Escrt-III: an endosome-associated heterooligomeric protein complex required for mvb sorting. Dev. Cell 3, 271-282.

Ghazi-Tabatabai, S., Saksena, S., Short, J.M., Pobbati, A.V., Veprintsev, D.B., Crowther, R.A., Emr, S.D., Egelman, E.H., and Williams, R.L. (2008). Structure and disassembly of filaments formed by the ESCRT-III subunit Vps24. Structure 16, 1345-1356.

Heuck, A. P., and Johnson, A. E. (2005). "Membrane Recognition and Pore Formation by Bacterial Pore-Forming Toxins" in Protein-Lipid Interactions (L. K. Tamm, editor), Wiley-VHC Weinheim, pp. 163-186.
Johnson, A.E., Adkins, H.J., Matthews, E.A., and Cantor, C.R. (1982). The Distance Moved by Transfer RNA During Translocation from the A Site to the P Site on the Ribosome. J. Mol. Biol. 156, 113-140.
Johnson, A.E. (2005). Fluorescence approaches for determining protein conformations, interactions and mechanisms at membranes. Traffic 6, 1078-1092.
Lata, S., Roessle, M., Solomons, J., Jamin, M., Göttlinger H.G., Svergun, D.I., and Weissenhorn W. (2008). Structural basis for Autoinhibition of ESCRT-III CHMP3. J. Mol. Biol. 378, 816-825.
Mutucumarana, V. P., Duffy, E. J., Lollar, P., and Johnson, A. E. (1992). The Active Site of Factor IXa Is Located Far Above the Membrane Surface and Its Conformation Is Altered Upon Association with Factor VIIIa. A Fluorescence Study. J. Biol. Chem. 267, 17012-17021
Muzioł T, Pineda-Molina E, Ravelli RB, Zamborlini A, Usami Y, Göttlinger H, and Weissenhorn W. (2006). Structural basis for budding by the ESCRT-III factor CHMP3. Dev. Cell 10, 821-830.
Ramachandran, R., Tweten, R. K., and Johnson, A. E. (2004). Membrane-dependent conformational changes initiate cholesterol-dependent cytolysin oligomerization and intersubunit beta-strand alignment. Nat. Struct. Mol. Biol. 11, 697-705.
Shatursky, O., Heuck, A.P., Shepard, L.A., Rossjohn, J., Parker, M.W., Johnson, A.E., and Tweten, R.K. (1999). The mechanism of membrane insertion for a cholesterol-dependent cytolysin: a novel paradigm for pore-forming toxins. Cell 99, 293-299.
Teis, D., Saksena, S., and Emr, S.D. (2008). Ordered assembly of the ESCRT-III complex on endosomes is required to sequester cargo during MVB formation. Dev. Cell 15, 578-589.
Teo, H., Perisic, O., González, B., and Williams, R. L. (2004). ESCRT-II, an endosome-associated complex required for protein sorting: crystal structure and interactions with ESCRT-III and membranes. Dev. Cell 7, 559-569.
Turcatti, G., Nemeth, K., Edgerton, M.D., Meseth, U., Talabot, F., Peitsch, M., Knowles, J., Vogel, H., and Chollet, A. (1996). Probing the structure and function of the tachykinin neurokinin-2 receptor through biosynthetic incorporation of fluorescent amino acids at specific sites. J. Biol. Chem. 271, 19991-19998.
Woolhead, C. A., McCormick, P. J., and Johnson, A. E. (2004). Nascent membrane and secretory proteins differ in FRET-detected folding far inside the ribosome and in their exposure to ribosomal proteins. Cell 116, 725-736.
Yorikawa, C., Shibata, H., Waguri, S., Hatta, K., Horii, M., Katoh, K., Kobayashi, T., Uchiyama, Y., and Maki, M. (2005). Human CHMP6, a myristoylated ESCRT-III protein, interacts directly with an ESCRT-II component EAP20 and regulates endosomal cargo sorting. Biochem. J. 387, 17-26.

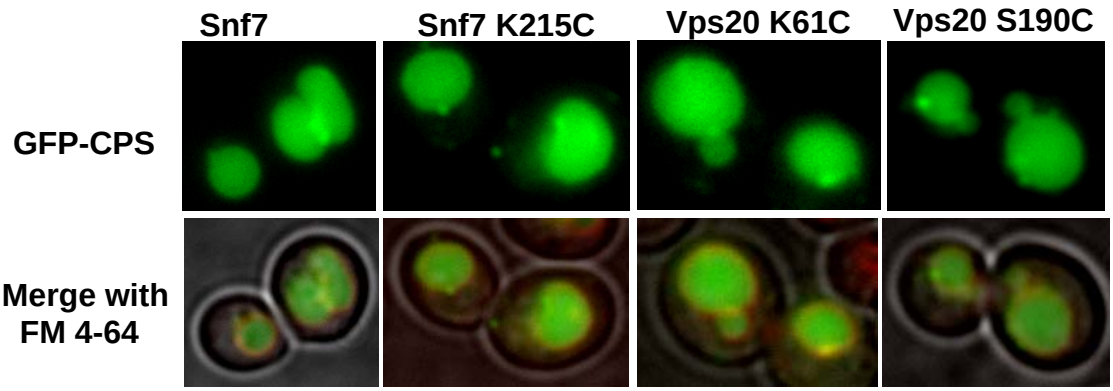

Figure S1. **Cysteine substitutions and CPS sorting.** GFP-CPS accumulates in the vacuolar lumen of *snf7Δ* cells expressing the Snf7 cysteine mutants (Snf7 E81C & Snf7 K215C; left two panels). Also, GFP-CPS is sorted normally to the vacuolar lumen in *vps20Δ* cells expressing the Vps20 cysteine mutants (Vps20 K61C & Vps20 S190C; right two panels). The FM4-64 dye preferentially localizes in the limiting membrane of the vacuole.

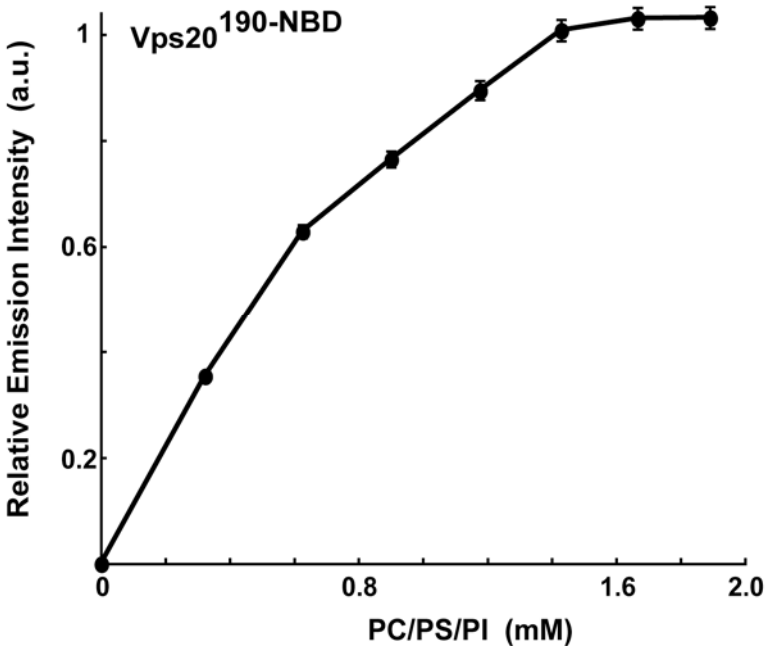

Figure S2. Vps20 binding to membranes. Titration of 800 nM Vps20$^{190\text{-NBD}}$ with liposomes reveals that fluorescence-detected (λ_{em} = 530 nm) binding is complete after addition of 1.5 mM PC/PS.

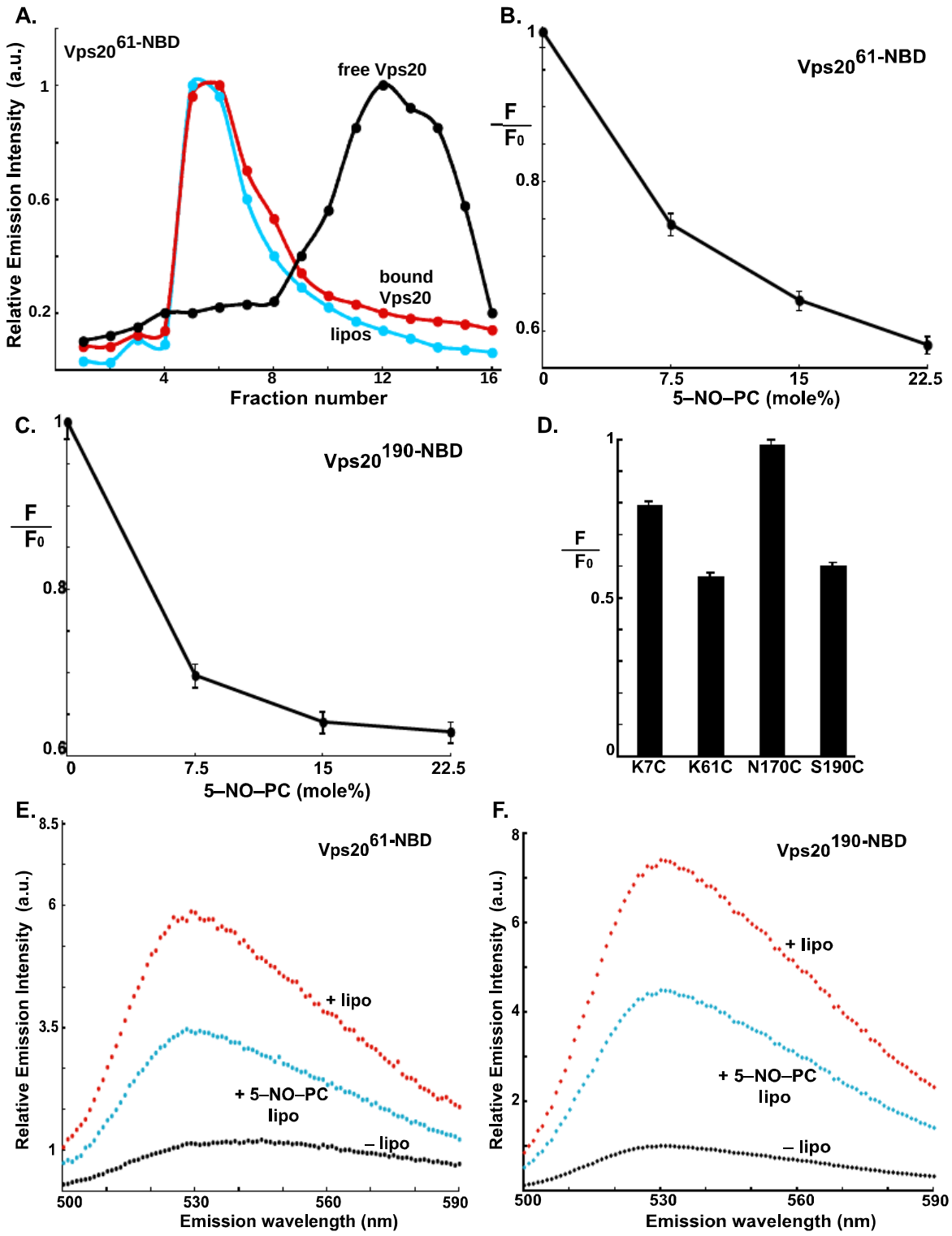

Figure S3. Vps20 exposure to nonpolar core of membrane. (A) Sepharose CL-2B chromatography of 1 μM Vps20$^{61\text{-NBD}}$ that had been preincubated with either 1.5 mM liposomes (77.5 mole% PC/PS/PI/22.5 mole% 5-NO-PC) (red) or

no liposomes (black). Protein was detected by NBD emission intensity and liposomes by light scattering (cyan). The elution profile of liposomes that were not exposed to protein was identical to the profile shown here (data not shown). NBD emission intensities (F; λ_{ex} = 468, λ_{em} = 530 nm) of 1 μM $Vps20^{61\text{-}NBD}$ (B) and 800 nM $Vps20^{190\text{-}NBD}$ (C) were measured after binding to excess **(**1.5 mM) liposomes containing different molar fractions of 5-NO-PC. F_0 = intensity of Vps20 bound to liposomes lacking 5-NO-PC. (D) The extents of quenching observed for the four Vps20 derivatives after addition of an excess of either PC/PS/PI vesicles (F_0) or 77.5 mole% PC/PS/PI/22.5 mole% 5-NO-PC vesicles (F). Fluorescence emission spectra of 1 μM $Vps20^{61\text{-}NBD}$ (E) and 800 nM $Vps20^{190\text{-}NBD}$(F) before (black) and after addition of excess (1.6 mM) liposomes, either PC/PS/PI (red) or 77.5 mole% PC/PS/PI/22.5 mole% 5-NO-PC (cyan).

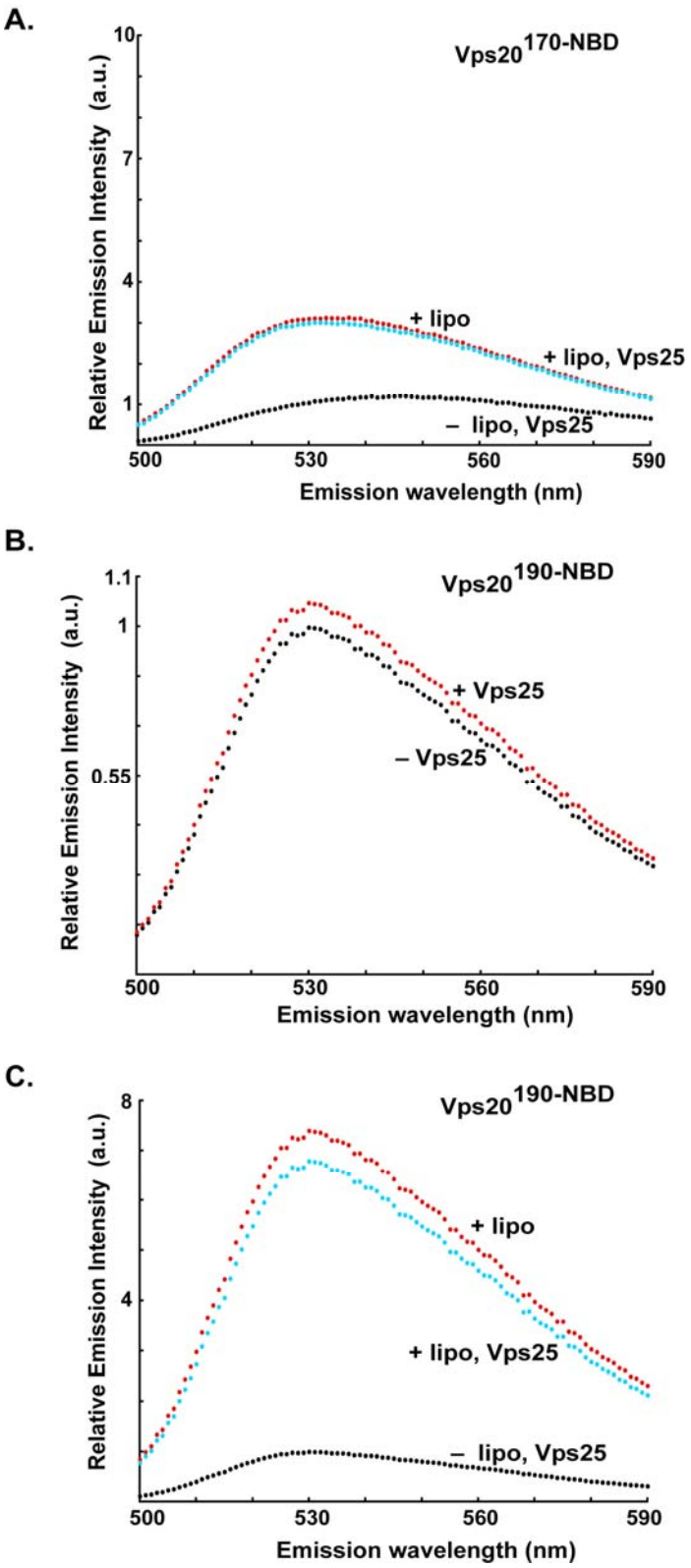

Figure S4. Vps20 interactions with Vps25. (A) Emission scans of 1 μM $Vps20^{170\text{-}NBD}$ are shown in HBS buffer (black), after addition of excess (1.5 mM)

liposomes (red), and after the addition of 30 μM Vps25 to $Vps20^{170\text{-}NBD}$ preincubated with 1.5 mM liposomes (cyan). (B) Fluorescence emission scans of 800 nM $Vps20^{190\text{-}NBD}$ are shown in HBS buffer (black) and after addition of 30 μM Vps25 (red). (C) Emission scans of 800 nM $Vps20^{190\text{-}NBD}$ are shown in HBS buffer (black), after addition of excess **(**1.5 mM) liposomes (red), and after the addition of 30 μM Vps25 to $Vps20^{190\text{-}NBD}$ preincubated with 1.5 mM liposomes (cyan).

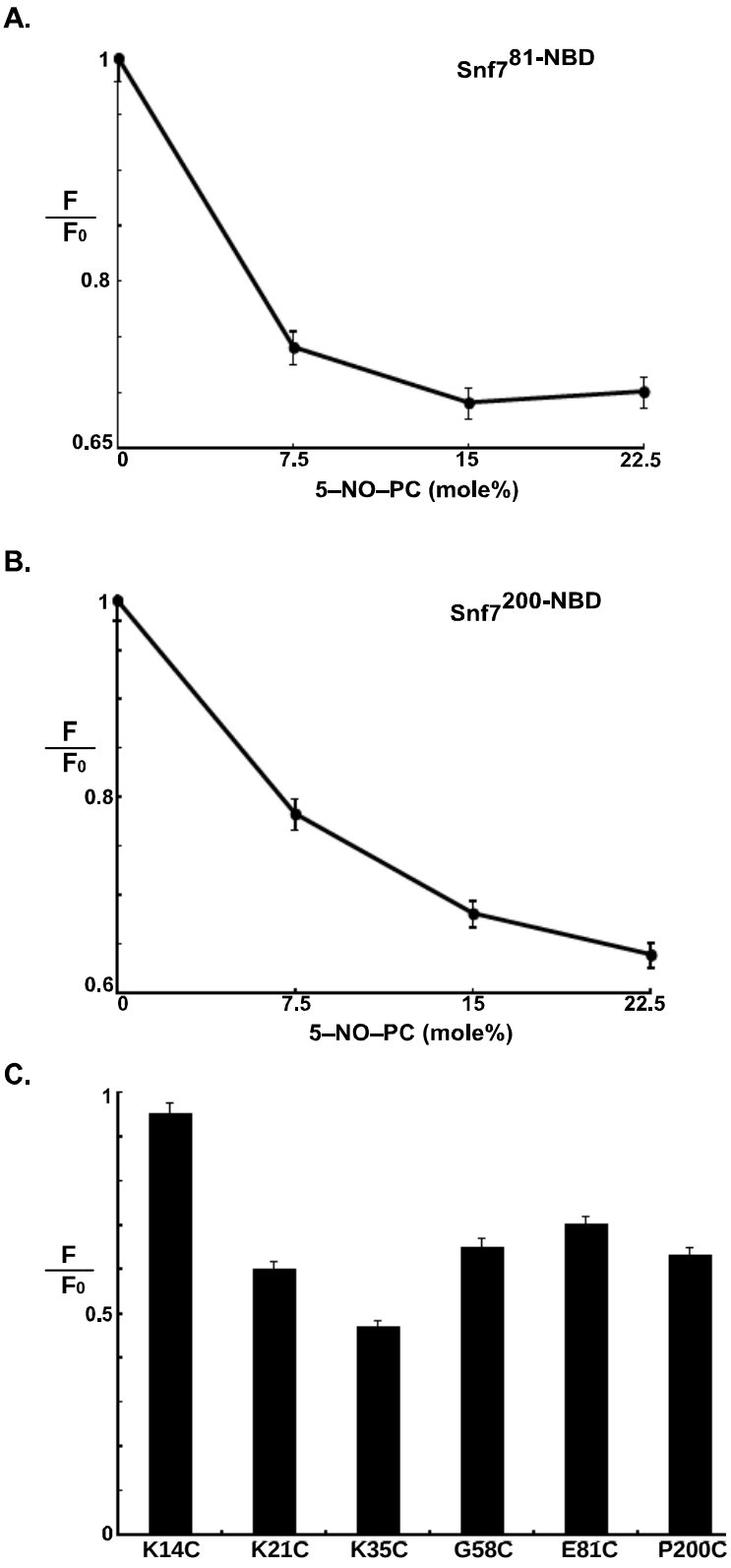

Figure S5. Snf7 exposure to lipid. NBD emission intensities (F; λ_{ex} = 468, λ_{em} = 530 nm) of 540 nM Snf7$^{81\text{-NBD}}$ (A) and 300 nM Snf7$^{200\text{-NBD}}$ (B) were measured

after binding to excess **(**1.5 mM) liposomes containing different molar fractions of 5-NO-PC. F_0 = intensity of Snf7 bound to liposomes lacking 5-NO-PC. (C) The extents of quenching observed for six Snf7 derivatives after addition of an excess of either PC/PS/PI vesicles (F_0) or 77.5 mole% PC/PS/PI/22.5 mole% 5-NO-PC vesicles (F).

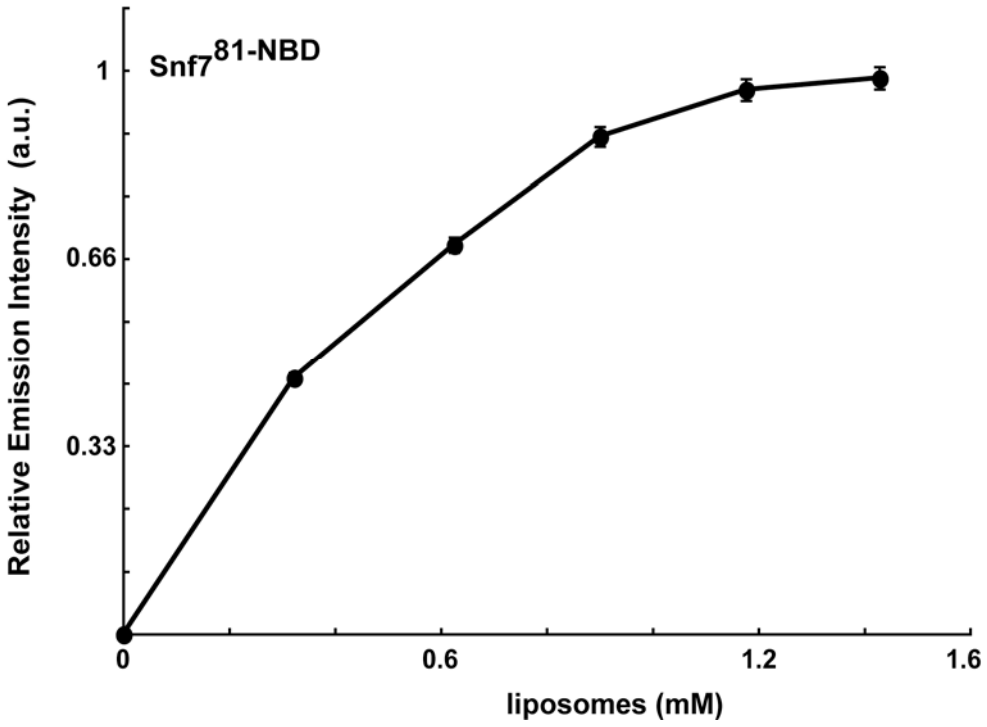

Figure S6. PC/PS/PI titration of Snf7$^{81\text{-NBD}}$. Titration of 540 nM Snf7$^{81\text{-NBD}}$ with liposomes reveals that fluorescence-detected (λ_{em} = 530 nm) binding is complete after addition of 1.5 mM PC/PS/PI.

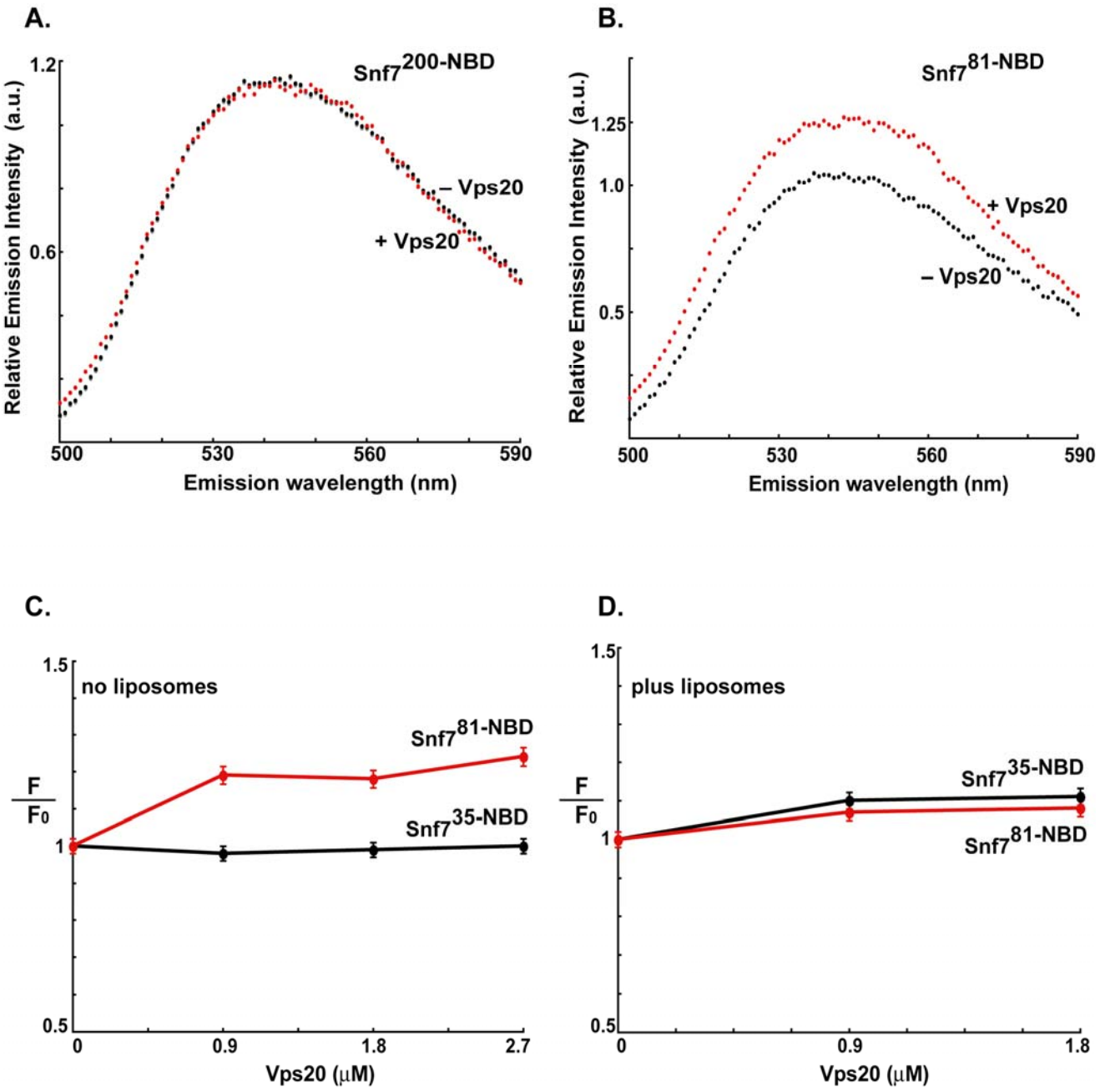

Figure S7. Vps20 binding to membrane-bound Snf7. Fluorescence emission spectra of 300 nM Snf7$^{200\text{-NBD}}$ (A) and 540 nM Snf7$^{81\text{-NBD}}$ (B) before (black) and after (red) addition of Vps20. Titration (λ_{em} = 530 nm) of 1 μM Snf7$^{35\text{-NBD}}$ (black) and 540 nM Snf7$^{81\text{-NBD}}$ (red) with Vps20 either before (C) or after incubation with 1.5 mM PC/PS/PI.

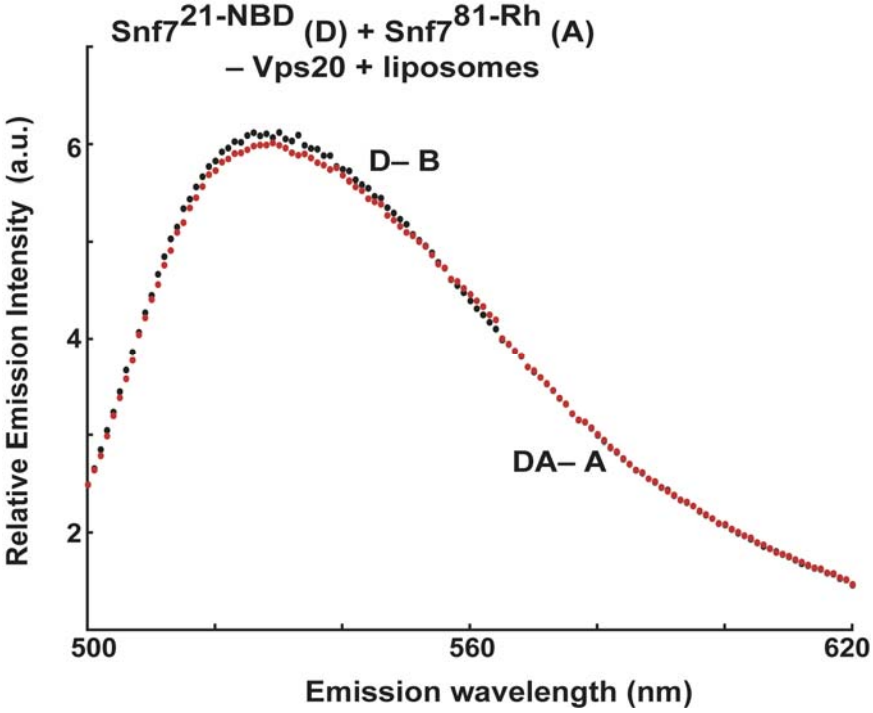

Figure S8. **Vps20 dependence of FRET.** The normalized net D (black) and DA (red) emission spectra of samples containing 530 nM $Snf7^{21\text{-}NBD}$, 4.2 μM $Snf7^{81\text{-}Rh}$, and 1.5 mM PC/PS/PI, but no Vps20.

```
Vps20  M--GQKSSKV--HITKTDRAILEVKRSKDEIHKFTRRTDNLILVEKSQLKDLIRKNPENYKSNMKVRFLLKRI
Snf7   MWSSLFGWTS-SNAKNKESPTKAIVRLREHINLLSKKQSHLRTQITNQ-ENEARIFLTK-GNKVMAKNALKKK
Vps24  M--DYIKKAI-WGPDPKEQQRRIRSVLRKNGRNIEKSLRELTVLQNKT-QQLIKKSAKK-NDVRTVRLYAKEL
Vps2   M--SLFEWVFGKNVTPQERLKKNQRALERTQRELEREKRKLELQDKKL-VSEIKKSAKN-GQVAAAKVQAKDL

Vps20  HYQEHLLQQASDQLINLENMVSTLEFKMVEKQFINGLKNGNEILKKLNK--EFSNVDELMDDVQDQIAYQNEI
Snf7   KTIEQLLSKVEGTMESMEQQLFSIESANLNLETMRAMQEGAKAMKTIHSGLDIDKVDETMDEIREQVELGDEI
Vps24  YQINKQYDRMYTSRAQLDSVRMKIDEAIRMNTLSNQMADSAGLMREVNSLVRLPQLRNTMIELEKELMKSGII
Vps2   VRTRNYIQKFDNMKAQLQAISLRIQAVRSSDQMTRSMSEATGLLAGMNRTMNLPQLQRISMEFEKQSDLMGQR

Vps20  NETLSRSLVGTSN--YEDDLDKELDALESELNPE---KMNNAKVANMP---STEGLPSLPQGEQTEQKER---
Snf7   SDAISRPLITGANEVDEDELDEELDMLAQENANQETSKIVNNNVNAAPISENKVSLPSVPSNKIKQSENSVKD
Vps24  SEMVDDTMESVGD--VGEEMDEAVDEEVNKIVEQ-YTNEKFKNVDQVP----TVELAANEEEQEIPDEKV---
Vps2   QEFMDEAIDNVMG--DEVDEDEEADEIVNKVLDE-IGVDLNSQLQSTP--QNLVSNAPIAETAMGIPEPIGAG

Vps20  EEFATEERSDTKEPLALLS-----
Snf7   GEEEEDEEDEDEKALRELQAEMGL
Vps24  DEEADRMVNEMRERLRALQN----
Vps2   SEFHGNPDDDLQARLNTLKKQT--
```

Figure S9. Sequence alignment of ESCRT-III proteins. Sequence alignment of the different ESCRT-III proteins showing the well conserved proline residues (highlighted in magenta) that are found at the junction of α5 and the loop leading to α6. The residues in α4 and the loop linking α3 and α4 that are critical for Vps24 filament formation in vitro are highlighted in blue. The corresponding residues in Snf7 that were mutated to analyze their effect on Snf7 oligomerization are also highlighted in blue.

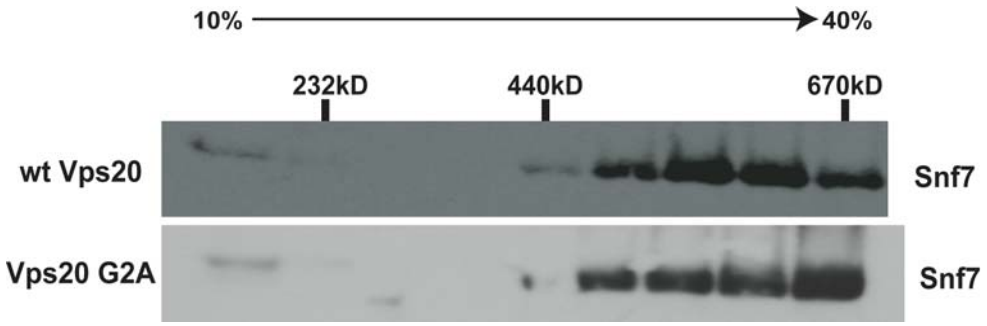

Figure S10. Vps20 G2A mutant can nucleate Snf7 oligomerization. Endosome (P13) fractions prepared from *vps4Δvps20Δ* cells expressing either wt Vps20 (top panel) or the G2A mutant of Vps20 were detergent solubilized, and analyzed using glycerol velocity gradients. The different fractions were analyzed by SDS-PAGE and immunoblotted using antibodies specific for Snf7.

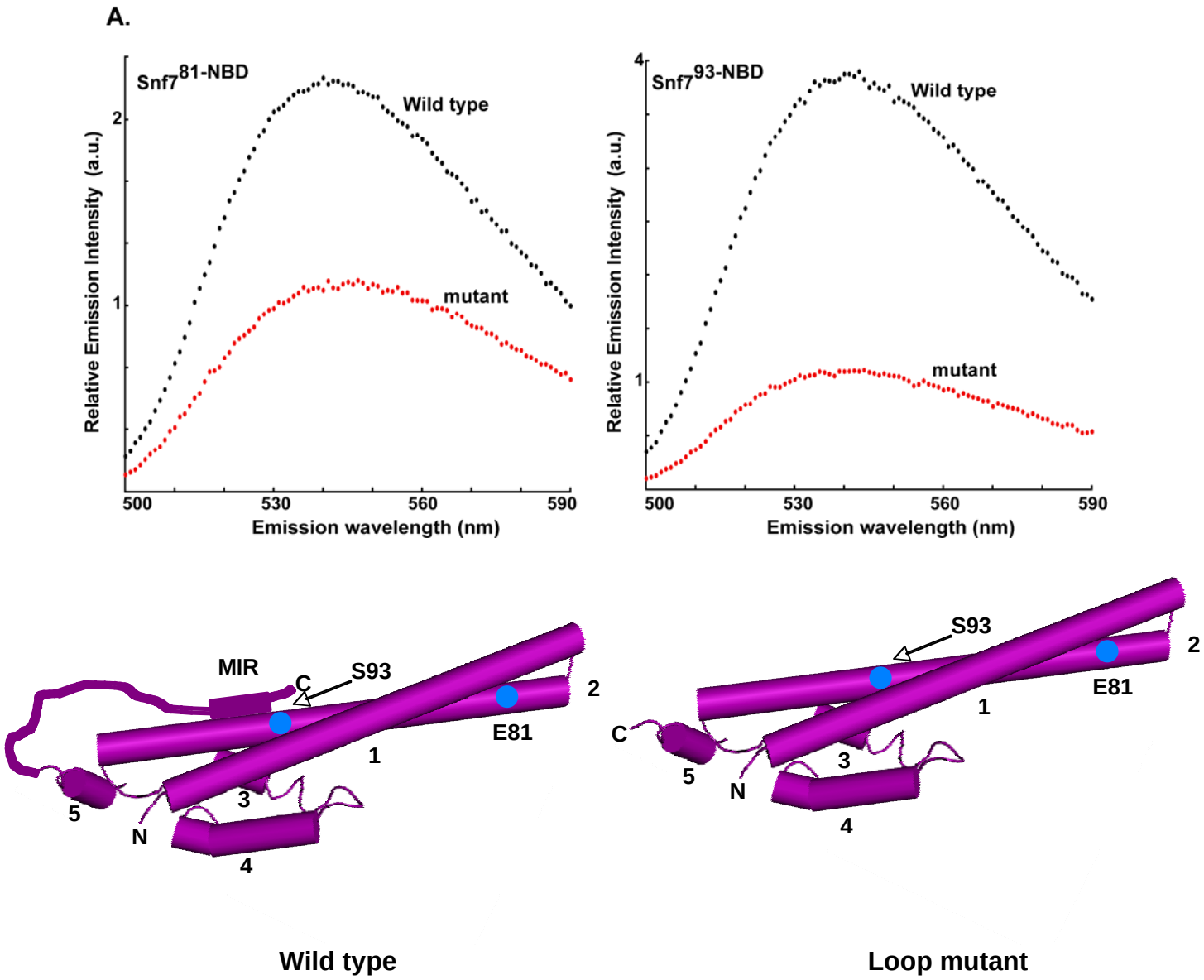

Figure S11. **NBD emission intensity profiles of Snf7 mutants.** Left panel: Fluorescence emission spectra of 540 nM Snf7$^{81\text{-NBD}}$ and 500 nM Snf7ΔMIR$^{81\text{-NBD}}$ in HBS buffer. Right panel: Fluorescence emission spectra of 300 nM Snf7$^{93\text{-NBD}}$ and 320 nM Snf7ΔMIR$^{93\text{-NBD}}$ in Buffer D. Also shown are the cartoon representations of the water-soluble hVps24 monomer (as in Fig. 1F) with (left) and without (right) the autoinhibitory helix α6 (MIR) and showing the locations of the probes used in Snf7 experiments (cyan).

Table S1. FRET efficiencies

Donor (D)	Acceptor (A)	Liposomes	Vps20	% FRET efficiency
$Snf7^{81\text{-}NBD}$	$Snf7^{81\text{-}Rh}$	–	–	0
$Snf7^{81\text{-}NBD}$	$Snf7^{81\text{-}Rh}$	+	–	10 (+/- 3%)
$Snf7^{81\text{-}NBD}$	$Snf7^{81\text{-}Rh}$	+	+	28 (+/- 4%)
$Snf7^{81\text{-}NBD}$	$Snf7^{81\text{-}Rh}$	+	$Vps20^{PW}$	4 (+/- 2%)
$Snf7^{21\text{-}NBD}$	$Snf7^{81\text{-}Rh}$	–	–	0
$Snf7^{21\text{-}NBD}$	$Snf7^{81\text{-}Rh}$	+	–	2 (+/- 2%)
$Snf7^{21\text{-}NBD}$	$Snf7^{81\text{-}Rh}$	+	+	12 (+/- 4%)
$Snf7^{21\text{-}NBD}$	$Snf7^{21\text{-}Rh}$	–	–	0
$Snf7^{21\text{-}NBD}$	$Snf7^{21\text{-}Rh}$	+	–	6 (+/- 3%)
$Snf7^{21\text{-}NBD}$	$Snf7^{21\text{-}Rh}$	+	+	23 (+/- 6%)
$Snf7^{PW\ 81\text{-}NBD}$	$Snf7^{PW\ 81\text{-}Rh}$	–	–	0
$Snf7^{PW\ 81\text{-}NBD}$	$Snf7^{PW\ 81\text{-}Rh}$	+	–	0
$Snf7^{PW\ 81\text{-}NBD}$	$Snf7^{PW\ 81\text{-}Rh}$	+	+	1 (+/- 2%)

The measured maximal FRET efficiencies for the different donor-acceptor pairs in samples containing different ESCRT-III components.